

## Quasilocal critical nature of cooperative paramagnetic fluctuations in CaRuO<sub>3</sub> metal

J. Gunasekera,<sup>1</sup> L. Harriger,<sup>2</sup> T. Heitmann,<sup>3</sup> A. Dahal,<sup>1</sup> H. Knoll,<sup>1</sup> and D. K. Singh<sup>1,\*</sup>

<sup>1</sup>*Department of Physics and Astronomy, University of Missouri, Columbia, Missouri 65211, USA*

<sup>2</sup>*NIST Center for Neutron Research, Gaithersburg, Maryland 20899, USA*

<sup>3</sup>*University of Missouri Research Reactor, University of Missouri, Columbia, Missouri 65211, USA*

(Received 2 November 2014; published 8 June 2015)

We report the observation of cooperative paramagnetic fluctuations of Ru<sup>4+</sup> spins that coexist with the non-Fermi-liquid state in CaRuO<sub>3</sub> perovskite below  $T \simeq 21$  K. Detailed electrical, magnetic, and neutron scattering measurements reveal that the Ru<sup>4+</sup> ions reside in magnetic-field-independent random domains with dynamic properties that are reminiscent of the cooperative paramagnetic fluctuations. The linear ( $E/T$ ) scaling of the dynamic susceptibilities and divergence of the mean relaxation time as  $T \rightarrow 0$  K suggest a quasilocal critical nature of the spin fluctuations. We argue that the non-Fermi-liquid behavior arises due to the quantum critical nature of the cooperative paramagnetic fluctuations in CaRuO<sub>3</sub>.

DOI: [10.1103/PhysRevB.91.241103](https://doi.org/10.1103/PhysRevB.91.241103)

PACS number(s): 71.10.Hf, 71.27.+a, 75.40.-s, 78.70.Nx

The presence or absence of the Fermi-liquid behavior in perovskite materials holds strong promise in understanding the exotic electronic properties that often accompany low temperature, such as unconventional superconductivity and the quantum criticality [1–3]. In addition to the fundamental understanding, ruthenate perovskites of the form ARuO<sub>3</sub>, where  $A = \text{Sr}$  or  $\text{Ca}$ , have possible implications in the technologically important spintronics devices, especially in the thin film form where magnetic properties can easily be manipulated for desired applications as the spin-polarized tunnel junctions [4,5]. While SrRuO<sub>3</sub> is ferromagnetic ( $T_c \simeq 160$  K), the magnetic nature of CaRuO<sub>3</sub> is still a subject of debate [5–14]. Both compounds, however, exhibit interesting non-Fermi-liquid (NFL) behavior at low temperature ( $T \leq 40$  K) [11,15–17]. CaRuO<sub>3</sub>, in fact, undergoes a crossover transition at  $T \simeq 30$  K, which separates two NFL states with distinct power-law exponents of electrical resistivity [17]. In a more recent work, Schneider *et al.* have claimed the observation of the quantum oscillations, implying a Fermi-liquid ground state, in a thin film of CaRuO<sub>3</sub> at very low temperature  $T \leq 1.5$  K; thus, challenging the present understanding of this material [18]. The unusual combination of the absence of magnetic order and the anomalous non-Fermi-liquid properties makes CaRuO<sub>3</sub> an archetypal perovskite for the exploration of the quantum magnetism [19].

In this Rapid Communication, we address the important question of the dynamic magnetism and its relation to the non-Fermi-liquid behavior in CaRuO<sub>3</sub> using detailed electrical, magnetic, and neutron scattering measurements on a high quality polycrystalline sample of CaRuO<sub>3</sub>. Here, we show that the underlying magnetism is depicted by the quantum-mechanical fluctuations of Ru<sup>4+</sup> spins, confined to field-independent random domains that form a cooperative paramagnetic state at low temperature. The dynamic structure factor, which increases significantly below  $T \leq 21$  K, manifests a linear ( $E/T$ ) scaling, implying the Curie-Weiss type fluctuations with temperature as the most relevant parameter. Moreover, the linear dynamic scaling in conjunction with the divergence of the spin fluctuations mean relaxation time as  $T \rightarrow 0$  K

suggest the existence of a “quasilocal” critical behavior in the system. Finally, we argue that the quantum spin fluctuations arising due to the dynamic cooperative paramagnetism is at the core of the low temperature ( $T \leq 30$  K) non-Fermi-liquid properties in CaRuO<sub>3</sub>.

CaRuO<sub>3</sub> is a pseudocubic metallic perovskite, which crystallizes in the orthorhombic structure ( $Pnma$  crystallographic group) with lattice parameters of  $a = 5.545$  Å,  $b = 7.673$  Å, and  $c = 5.398$  Å [8,9,11,20]. The octahedral crystalline electric field splits the fivefold degeneracy of Ru  $4d^4$  into  $(t_{2g})^4$  and empty  $e_g$ , thus resulting in a low-spin electronic configuration [7,10]. <sup>17</sup>O NMR investigation of the spin dynamics in Sr<sub>1-x</sub>Ca<sub>x</sub>RuO<sub>3</sub> claimed robust ferromagnetic fluctuations of Ru<sup>4+</sup> spins for all doping percentages [21]. The inevitable introduction of disorder due to the chemical doping complicates such universal analysis [22]. Heat capacity measurement on single crystal CaRuO<sub>3</sub> has revealed a logarithmic temperature dependence with a reasonably heavy electron characteristic, specific heat coefficient of 73 mJ/mol K<sup>2</sup>, at low temperature [11,23]. These observations are reminiscent of the local quantum critical phenomenon, usually found in the intermetallic heavy fermion systems [24,25]. It is long suspected that the non-Fermi-liquid behavior in CaRuO<sub>3</sub> culminates in a quantum critical state as  $T \rightarrow 0$  K, but has never been observed.

The high purity polycrystalline samples of CaRuO<sub>3</sub> were synthesized by conventional solid-state reaction method using ultrapure ingredients of RuO<sub>2</sub> and CaCO<sub>3</sub>. Starting materials were mixed in stoichiometric composition, with 10% extra RuO<sub>2</sub> to compensate for their rapid evaporation, palletized and sintered at 950° for three days. The furnace cooled samples were ground, palletized, and sintered at 1000° for another three days. Resulting samples were characterized using Siemens D500 powder x-ray diffractometer. The x-ray diffraction (XRD) data were refined using the FULLPROF suite for the Rietveld structure profile refinement. As shown in Fig. S1 of the Supplementary Material [26], every single peak of the XRD pattern was identified with the  $Pnma$  orthorhombic structure of CaRuO<sub>3</sub>. A four-probe technique was employed to measure electrical properties of CaRuO<sub>3</sub> using a closed-cycle refrigerator cooled 9 T magnet with a measurement temperature range of 1.5–300 K. Detailed ac susceptibility measurements were

\*singhdk@missouri.edu

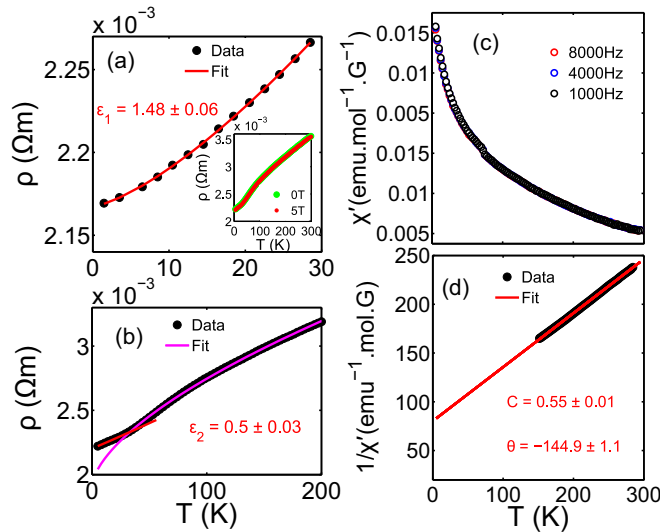


FIG. 1. (Color online) Electrical resistivity and magnetic measurements of  $\text{CaRuO}_3$ . (a) and (b) Electrical resistivity as a function of temperature, depicting two different non-Fermi-liquid states in low temperature (below  $T \simeq 30$  K) and high temperature ( $30 \text{ K} \leq T \leq 200$  K) regimes. The resistivity data is fitted using the power-law equation,  $\rho = T^\epsilon$ , with fitted value of  $\epsilon = 1.48(0.06)$  [Fig. 1(a)] and  $0.5(0.03)$  [Fig. 1(b)] in low and high temperature regimes, respectively. Electrical resistivities as a function of temperature at different applied magnetic fields,  $H = 0$  and  $5$  T, are shown in the inset. No significant field effect on the electrical resistance is observed. (c) Static susceptibilities ( $\chi'$ ) at few characteristic frequencies are plotted as a function of temperature in this figure.  $\chi'$  is found to be independent of the ac frequency. We also observe a small but sharp cusp in  $\chi'$  at  $T \simeq 80$  K. While the origin of this cusp is not yet clear, no magnetic order was detected in the elastic neutron scattering measurements below this temperature. (d) High temperature ( $T \geq 150$  K) inverse static susceptibility data, at very low frequency ( $\simeq 10$  Hz), is fitted using the Curie-Weiss (CW) law.

performed using a physical properties measurement system with a temperature range of 2–300 K. Neutron scattering measurements were performed on 4.8 g pristine powder sample of  $\text{CaRuO}_3$  on the spin-polarized triple-axis spectrometer (SPINS) at the NIST Center for Neutron Research and on the thermal triple-axis spectrometer TRIAX at the Missouri University Research Reactor with fixed final neutron energies of 3.7 and 14.7 meV, respectively. At these fixed final energies, the spectrometers resolution (FWHM) were determined to be  $\simeq 0.16$  and 0.8 meV, respectively. Measurements on SPINS employed a cold Be filter followed by a radial collimator and the focused analyzer. Measurements were also performed in applied field with the sample mounted at the end of a 1 K stick in a 10 T vertical field magnet.

The temperature dependence of the electrical resistivity is shown in Figs. 1(a) and 1(b). The experimental data are well described by a power-law expression,  $\rho \propto T^\epsilon$ . The fitting parameter  $\epsilon$  is found to exhibit two different values:  $\epsilon_1 = 1.48(0.06)$  below  $T \simeq 30$  K and  $\epsilon_2 = 0.5(0.03)$  in  $30 \text{ K} \leq T \leq 200$  K; illustrating two different non-Fermi-liquid states above and below the crossover temperature of 30 K. These results are consistent with the previous observations on high

quality specimens of  $\text{CaRuO}_3$  [8,11,16,17]. Surprisingly, the resistivity is found to be independent of the magnetic field application (up to 9 T field), as shown in the inset of Fig. 1(a). Measurements of the static magnetic susceptibility ( $\chi'$ ) reveal two interesting behaviors [Fig. 1(c)]: a small cusp around  $T \simeq 80$  K and the divergence of  $\chi'$  at low temperature. A similar phenomenon (the cusp at  $T \simeq 80$  K) was previously attributed to the onset of a long-range magnetic order [13]. However, no signature of any magnetic order is observed in the elastic neutron scattering measurements (see Fig. S2 in the Supplemental Material) [26]. It is possible that this anomalous observation is associated to a weak structural transition. Bulk static susceptibilities, including the cusp at  $T \simeq 80$  K, are also found to be independent of ac measurement frequency, hence ruling out the occurrence of the spin freezing or a short-range static order in the system. The divergence in  $\chi'$  at low temperature is most likely arising due to the quantum critical nature of the cooperative paramagnetic fluctuations, as explained later.

Fitting of the high temperature ( $T \geq 150$  K) static susceptibility data using the Curie-Weiss law  $\chi' = C/(T - \theta)$ , Fig. 1(d), yields  $\theta = -144.9$  K and  $C = 0.55$ . Under the mean-field approximation, the Curie-Weiss temperature of  $-144.9$  K implies an antiferromagnetic interaction of strength  $J \simeq 6.8$  meV for the effective moment of  $2.56\mu_B$  per ruthenium ion (estimated from the CW constant  $C$ ) [27]. Despite a reasonably large exchange constant and a near full moment value in the Curie-Weiss regime, the absence of magnetic order is perplexing. Recent reports, particularly on the thin film of  $\text{CaRuO}_3$ , suggest that the system is on the verge of attaining an ordered state. Another possibility is that strong spin fluctuations cause destabilization to a nascent order, thus preventing it from developing a long-range magnetic order. We have further investigated the dynamic properties to explore this possibility.

Plots of the dynamic susceptibilities ( $\chi''$ ) as functions of temperature and frequency are shown in Figs. 2(a) and 2(b), respectively. Unlike the static susceptibilities, the dynamic susceptibilities exhibit strong frequency dependence. In an interesting observation, we notice a significant enhancement in  $\chi''$  as the strength of ac frequency increases from 10 to  $10^4$  Hz [Fig. 2(a)]. The dynamic susceptibilities tend to diverge as the measurement temperature is reduced below  $T \simeq 25$  K. Coincidentally, this is also very close to the crossover temperature ( $\sim 30$  K) separating two non-Fermi-liquid states at low temperature [17]. The frequency dependence of  $\chi''$  hints of significant spin fluctuations in  $\text{CaRuO}_3$ . The dynamic behavior is also reflected in the inelastic neutron scattering measurement where the dynamic structure factor, depicted by the neutron intensity count, at  $Q = 1.06 \text{ \AA}^{-1}$  and at an energy transfer of  $\Delta E = 0.8$  meV exhibits significant enhancement above the background at low temperature, Fig. 2(c). Experimental data is fitted using a power law,  $I \propto (1 - T/T_0)^{-2\beta}$ , where  $T_0$ , associated to the onset of dynamic magnetic structure factor, is found to be 21 K. The temperature vs frequency (energy) behavior, describing the dynamic response of  $\text{Ru}^{4+}$  spins to the external tuning parameters of frequency and temperature, is described in a comprehensive contour plot in Fig. 2(d). Clearly, the spin fluctuations get stronger as the

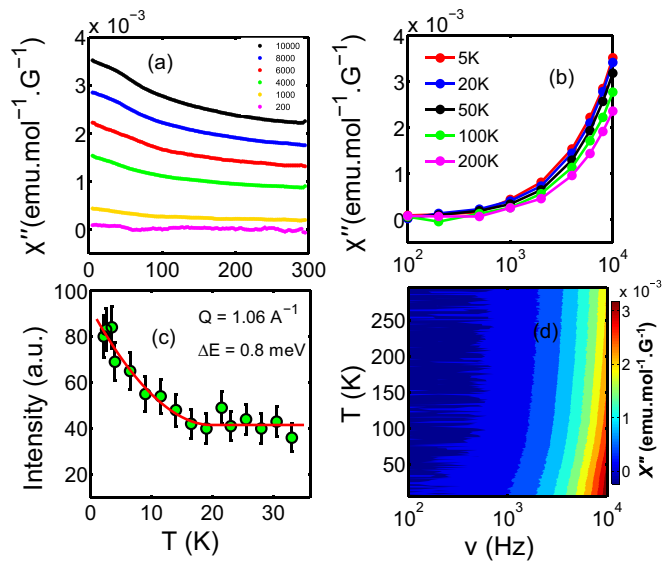


FIG. 2. (Color online) Dynamic magnetic properties of  $\text{CaRuO}_3$ . (a) Dynamic ac susceptibilities ( $\chi''$ ) are plotted as a function of temperature at few characteristic frequencies. Clearly, the system exhibits significant dynamic response to the ac frequency ( $10$ – $10^4$  Hz), which becomes stronger below  $T \simeq 25$  K. (b)  $\chi''$  as a function of ac frequency at a few different temperatures are shown in this figure. We immediately notice the divergence in  $\chi''$  at high frequency at any temperature. (c) Inelastic neutron scattering intensity at  $Q = 1.06 \text{ \AA}^{-1}$  and at an energy transfer of  $\Delta E = 0.8$  meV is plotted as a function of temperature in this figure. The error bar represents one standard deviation. Inelastic intensity, which exhibits significant enhancement below  $T \simeq 21$  K, is described by a power-law equation, yielding  $\beta = 0.45$  (see text for details). (d)  $T$  vs  $\nu$  contour map of  $\chi''$  sums up the dynamic behavior of magnetic fluctuations as inferred from the ac susceptibility measurements.

temperature is reduced, indicating quantum characteristics of the behavior.

In order to elucidate the quantum-mechanical nature of the spin fluctuations in  $\text{CaRuO}_3$ , detailed inelastic neutron scattering measurements were performed on SPINS as a function of energy with a fixed final energy of  $3.7$  meV, yielding a resolution of  $\simeq 0.16$  meV. Inelastic data were collected at various fixed  $Q$  values between  $0.7$  and  $1.5 \text{ \AA}^{-1}$  and at various temperatures between  $T = 1$  and  $120$  K. Background corrected characteristic energy scans at selected  $Q$  values at  $T = 4.5$  K and at selected temperatures at  $Q = 1.06 \text{ \AA}^{-1}$  are plotted in Figs. 3(a)–3(d) and Figs. 3(e)–3(h), respectively. The magnetic nature of the quasielastic spectra is ascribed to the observed weakening of the peak intensity at higher  $Q$  and the weak spectral count above the background at high temperatures. Inelastic measurements were also performed in applied magnetic field but no significant or observable difference compared to the zero field data was detected at any temperature (illustrated in Fig. S3 of the Supplemental Material) [26].

Inelastic neutron scattering data were fitted using various relevant formulations to understand the dynamic properties of  $\text{Ru}^{4+}$  spins. The experimental data are found to be best described by a cooperative paramagnetic fluctuation model,

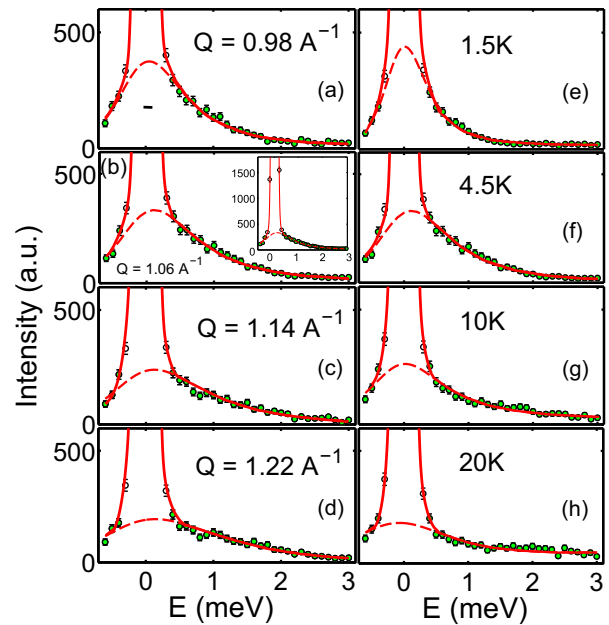


FIG. 3. (Color online) Inelastic neutron scattering measurements, carried out on SPINS, as a function of energy. (a)–(d) Characteristic energy scans at constant  $Q$  at  $T = 4.5$  K are plotted in these figures. The solid line represents the complete fitting profile of the background corrected experimental data due to Eq. (1), convoluted with the instrument resolution and consists of an elastic line (Gaussian) and a quasielastic function multiplied by the detailed balance factor. The quasielastic data (dashed lines) are well described by a Lorentzian-squared line shape, emphasizing the cooperative paramagnetic nature of  $\text{Ru}^{4+}$  spins fluctuation in the system (see text for details). As the absolute  $Q$  increases, the peaks become broader and weaker, suggesting a magnetic nature of fluctuation. (e)–(h) Energy scans at constant temperatures at  $Q = 1.06 \text{ \AA}^{-1}$  are plotted. The inelastic spectra become stronger as the measurement temperature is reduced. The error bar in all figures represents one standard deviation.

involving higher orders of Lorentzian function [28]:

$$I(Q, E) = e^{-(E/\Gamma_0)^2} + \left( \frac{\Gamma_1}{E^2 + \Gamma_1^2} \right)^\nu \frac{E/k_B T}{1 - e^{-E/k_B T}}, \quad (1)$$

where  $\Gamma_0$  and  $\Gamma_1$  are fitting parameters, related to the actual linewidths of the elastic and the quasielastic features, respectively. The solid line in Fig. 3 manifests the complete fitting profile of the experimental data due to Eq. (1), convoluted with the instrument resolution and consists of an elastic line (Gaussian) and a quasielastic function (higher order Lorentzian function) multiplied by the detailed balance factor. The best fit is obtained for  $\nu = 2$ , giving a Lorentzian-squared line shape of the quasielastic data. The width of the elastic line, FWHM of the Gaussian profile, remains resolution limited ( $\simeq 0.16$  meV) at all temperatures. The Lorentzian-squared line shape, arguably, manifests random fields arising from the impurities or the presence of magnetic domains or clusters in a system, for example, a spin glass or geometrically frustrated magnet [29]. The high purity of the sample rules out impurity as the underlying reason. The formation of small ferromagnetic domains, behaving as dynamic paramagnetic

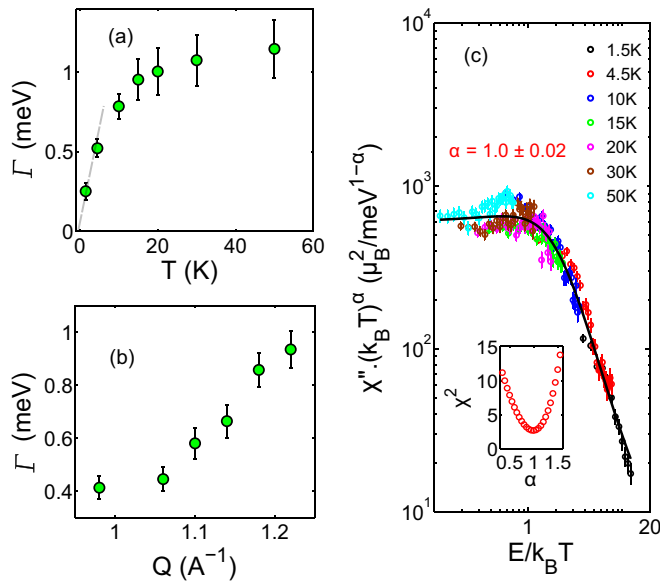


FIG. 4. (Color online)  $(E/T)$  scaling and the quantum critical nature of spin fluctuations. (a) Deconvoluted linewidth  $\Gamma$  ( $\propto 1/\tau$ ,  $\tau$ —mean relaxation time) is plotted as a function of temperature at  $Q = 1.06 \text{ \AA}^{-1}$ . The linewidth decreases significantly below  $T \simeq 25 \text{ K}$  and approaches zero as  $T \rightarrow 0 \text{ K}$ , suggesting the presence of quantum critical behavior in the system. The dashed line is used as a guide to the eye. (b) Deconvoluted  $\Gamma$  as a function of absolute  $Q$  at  $T = 4.5 \text{ K}$ . The linewidth increases as a function of increasing  $Q$ . (c)  $(E/T)$  scaling of the dynamic susceptibilities further confirm the role of temperature as the single most relevant parameter of the spin fluctuations, as expected for the cooperative paramagnetic phenomena. Scaling was tried for various different values of the exponent  $\alpha$ . However, the best fit, given by minimum  $\chi^2$ , is obtained for  $\alpha = 1.0$  (see inset).

clusters, of  $\text{Ru}^{4+}$  spins is a possible explanation for this unusual observation. At the same time, however, both elastic and inelastic measurements remain unaffected to the magnetic field application of strength up to 10 T [see Fig. S2(b) and Fig. S3 in the Supplemental Material] [26]. This is in stark contrast to the previous understanding that the system is “on the verge of the ferromagnetic instability” [9–11]. Rather, we argue that the magnetic ground state in  $\text{CaRuO}_3$  consists of field-independent domains that are strongly fluctuating as cooperative paramagnets. The cooperative paramagnetic fluctuations were previously used to describe a spin liquid type ground state in  $\text{Tb}_2\text{Ti}_2\text{O}_7$  [30].

Next, we investigate the quantum-mechanical nature of the cooperative spin fluctuations in  $\text{CaRuO}_3$ . As inferred from Figs. 3(e)–3(h), inelastic peaks become broader as the measurement temperature is increased. The quantitative estimation of the linewidth  $\Gamma$  due to the quasielastic fluctuations of  $\text{Ru}^{4+}$  ions, related to  $\Gamma_1$  via  $\Gamma = 2\Gamma_1\sqrt{(\sqrt{2}-1)}$ , suggests a significant slowing down of the mean relaxation time ( $\tau \propto 1/\Gamma$ ) below  $T \simeq 25 \text{ K}$ . The linewidth is further deconvoluted from the instrument resolution. In Fig. 4(a), we have plotted

deconvoluted  $\Gamma$  as a function of temperature. Clearly  $\Gamma$  tends to approach zero as  $T \rightarrow 0 \text{ K}$  [Fig. 4(a)], indicating the development of a quantum critical state in the system [31]. The estimated  $\Gamma$  is at least three times broader than the instrument resolution at different  $Q$  values, Fig. 4(b). More insight into the quantum-mechanical nature of the spin fluctuations is obtained by performing the scaling analysis of the dynamic spin susceptibility data in the form of  $\chi'' T^\alpha = f(E/T)$ , where  $\alpha$  is the dynamic scaling exponent [32]. The dynamic susceptibilities are extracted from the inelastic neutron data using standard neutron scattering intensity analysis, given by  $I = (1/\pi)\chi''/(1 - e^{-E/k_B T})$  [31]. The scaling plot of the dynamic susceptibilities is shown in Fig. 4(c). As illustrated in the inset of Fig. 4(c), the best overlap of the dynamic susceptibilities at different temperatures is obtained for the exponent  $\alpha = 1.0(0.02)$ . There are two important implications of this analysis: first, the linear  $(E/T)$  scaling reflects a Curie-Weiss type fluctuation, which is consistent with our argument that the cooperative paramagnetism is at the core of the observed spin fluctuations with temperature as the most relevant parameter [24,25]. Second, it suggests the existence of a quantum critical fixed point in  $\text{CaRuO}_3$ . While more research is needed, preferably on a single crystal specimen, to further understand the nature of the quantum critical fluctuations and the anisotropic properties, the cooperative nature of the paramagnetic fluctuations of  $\text{Ru}^{4+}$  domains makes it a quasilocal event.

We have performed detailed electrical, magnetic, and neutron scattering measurements on the high purity powder sample of  $\text{CaRuO}_3$  to investigate the spin dynamics and its correlation to the non-Fermi-liquid behavior. It is found that  $\text{Ru}^{4+}$  spins, residing in field-independent domains, exhibit strong paramagnetic fluctuations below  $T \simeq 21 \text{ K}$ , which is very close to the crossover temperature ( $\sim 30 \text{ K}$ ) separating two NFL phenomena at low temperature. The field-independent characteristic of magnetic domains can also be arising due to a coupling between the  $\text{Ru}^{4+}$  spin fluctuations and the orbital fluctuations. A recent report has suggested that the orbital fluctuations play a key role in the anomalous non-Fermi-liquid properties in  $\text{CaRuO}_3$  [33]. Further theoretical investigations are necessary to understand this. Nonetheless, the cooperative nature of the paramagnetic fluctuations lead to a dynamic ground state in  $\text{CaRuO}_3$ . As  $T \rightarrow 0 \text{ K}$ , the mean relaxation time of the paramagnetic fluctuations tends to become infinity. The divergence of the mean relaxation time in conjunction with the linear  $(E/T)$  scaling of the dynamic susceptibilities hints of a quasilocal critical behavior, coexisting with the non-Fermi-liquid state in this compound. These findings provide a new research arena to explore new quantum material where the cooperative paramagnetism leads to a fragile or nonmagnetic ground state, such as a quantum spin liquid [34].

We acknowledge support from the University of Missouri Research Board and IGERT research program, funded by NSF under Grant No. DGE-1069091.

[1] H. v. Lohneysen, A. Rosch, M. Vojta, and P. Wolfe, *Rev. Mod. Phys.* **79**, 1015 (2007).

[2] D. M. Broun, *Nat. Phys.* **4**, 170 (2008).

- [3] R. A. Cooper, Y. Wang, B. Vignolle, O. J. Lipscombe, S. M. Hayden, Y. Tanabe, T. Adachi, Y. Koike, M. Nohara, H. Takagi, Cyril Proust, and N. E. Hussey, *Science* **323**, 603 (2009).
- [4] K. S. Takahashi, A. Sawa, Y. Ishii, H. Akoh, M. Kawasaki, and Y. Tokura, *Phys. Rev. B* **67**, 094413 (2003).
- [5] S. Tripathi, R. Rana, S. Kumar, P. Pandey, R. S. Singh, and D. S. Rana, *Sci. Rep.* **4**, 3877 (2014).
- [6] J. M. Longo, P. M. Raccach, and J. B. Goodenough, *J. Appl. Phys.* **39**, 1327 (1968).
- [7] G. Cao, S. McCall, M. Shepard, J. E. Crow, and R. P. Guertin, *Phys. Rev. B* **56**, 321 (1997).
- [8] N. Kikugawa, L. Balicas, and A. P. Mackenzie, *J. Phys. Soc. Jpn.* **78**, 014701 (2009).
- [9] T. He and R. J. Cava, *J. Phys.: Condens. Matter* **13**, 8347 (2001).
- [10] I. I. Mazin and D. J. Singh, *Phys. Rev. B* **56**, 2556 (1997).
- [11] G. Cao, O. Korneta, S. Chikara, L. E. DeLong, and P. Schlottmann, *Solid State Commun.* **148**, 305 (2008).
- [12] P. Khalifah, I. Ohkubo, H. M. Christen, and D. G. Mandrus, *Phys. Rev. B* **70**, 134426 (2004).
- [13] I. Felner, I. Nowik, I. Bradaric, and M. Gospodinov, *Phys. Rev. B* **62**, 11332 (2000).
- [14] H. Mukuda, K. Ishida, Y. Kitaoka, K. Asayama, R. Kanno, and M. Takano, *Phys. Rev. B* **60**, 12279 (1999).
- [15] P. Kostic, Y. Okada, N. C. Collins, Z. Schlesinger, J. W. Reiner, L. Klein, A. Kapitulnik, T. H. Geballe, and M. R. Beasley, *Phys. Rev. Lett.* **81**, 2498 (1998).
- [16] Y. S. Lee, J. Yu, J. S. Lee, T. W. Noh, T.-H. Gimm, H.-Y. Choi, and C. B. Eom, *Phys. Rev. B* **66**, 041104(R) (2002).
- [17] L. Klein, L. Antognazza, T. H. Geballe, M. R. Beasley, and A. Kapitulnik, *Phys. Rev. B* **60**, 1448 (1999).
- [18] M. Schneider, D. Geiger, S. Esser, U. S. Pracht, C. Stingl, Y. Tokiwa, V. Moshnyaga, I. Sheikin, J. Mravlje, M. Scheffler, and P. Gegenwart, *Phys. Rev. Lett.* **112**, 206403 (2014).
- [19] A. Georges, L. deMedici, and J. Mravlje, *Annu. Rev. Condens. Matter Phys.* **4**, 137 (2013).
- [20] H. Kojitani, Y. Shirako, and M. Akaogi, *Phys. Earth Planet. Inter.* **165**, 127 (2007).
- [21] K. Yoshimura, T. Imai, T. Kiyama, K. R. Thurber, A. W. Hunt, and K. Kosuge, *Phys. Rev. Lett.* **83**, 4397 (1999).
- [22] L. Capogna, A. P. Mackenzie, R. S. Perry, S. A. Grigera, L. M. Galvin, P. Raychaudhuri, A. J. Schofield, C. S. Alexander, G. Cao, S. R. Julian, and Y. Maeno, *Phys. Rev. Lett.* **88**, 076602 (2002).
- [23] M. Shepard, S. McCall, G. Cao, and J. E. Crow, *J. Appl. Phys.* **81**, 4978 (1997).
- [24] A. Schroder, G. Aeppli, R. Coldea, M. Adams, O. Stockert, H.v. Löhneysen, E. Bucher, R. Ramazashvili, and P. Coleman, *Nature (London)* **407**, 351 (2000).
- [25] Q. Si, S. Rabello, K. Ingersent, and J. L. Smith, *Nature (London)* **413**, 804 (2001).
- [26] See Supplemental Material at <http://link.aps.org/supplemental/10.1103/PhysRevB.91.241103> for brief description of the synthesis process and neutron scattering measurements in applied magnetic field.
- [27] P. W. Anderson and H. Hasegawa, *Phys. Rev.* **100**, 675 (1955).
- [28] J. P. Wicksted, P. Boni, and G. Shirane, *Phys. Rev. B* **30**, 3655 (1984).
- [29] G. MacDougall, D. Gout, J. L. Zarestky, G. Ehlers, A. Podlesnyak, M. A. McGuire, D. Mandrus, and S. E. Nagler, *Proc. Natl. Acad. Sci.* **108**, 15693 (2011).
- [30] J. S. Gardner, S. R. Dunsiger, B. D. Gaulin, M. J. P. Gingras, J. E. Greedan, R. F. Kiefl, M. D. Lumsden, W. A. MacFarlane, N. P. Raju, J. E. Sonier, I. Swainson, and Z. Tun, *Phys. Rev. Lett.* **82**, 1012 (1999).
- [31] D. K. Singh, A. Thamizhavel, J. W. Lynn, S. Dhar, J. Rodriguez-Rivera, and T. Herman, *Sci. Rep.* **1**, 117 (2011).
- [32] M. A. Continentino, *Quantum Scaling in Many-Body Systems* (World Scientific, Singapore, 2001).
- [33] M. S. Laad, I. Bradarić, and F. V. Kusmartsev, *Phys. Rev. Lett.* **100**, 096402 (2008).
- [34] I. Mirebeau, I. N. Goncharenko, P. Cadavez-Peres, S. T. Bramwell, M. J. P. Gingras, and J. S. Gardner, *Nature (London)* **420**, 54 (2002).